2017-01-01

# A tale of two gyres: Contrasting distributions of dissolved cobalt and iron in the Atlantic Ocean during an Atlantic Meridional Transect (AMT-19)

Rachel U. Shelley

Neil J. Wyatt

Glenn A. Tarran

Andrew P. Rees

Paul J. Worsfold *School of Geography, Earth and Environmental Sciences*

et al. *See next page for additional authors*

# A tale of two gyres: Contrasting distributions of dissolved cobalt and iron in the Atlantic Ocean during an Atlantic Meridional Transect (AMT-19)

**R.U. Shelley, N.J. Wyatt, G.A. Tarran, A.P. Rees, P.J. Worsfold, M.C. Lohan**

ABSTRACT

Cobalt (Co) and iron (Fe) are essential for phytoplankton nutrition, and as such constitute a vital link in the marine biological carbon pump. Atmospheric deposition is an important, and in some places the dominant, source of trace elements (TEs) to the global ocean. Dissolved cobalt (dCo) and iron (dFe) were determined along an Atlantic Meridional Transect (*AMT*-19; Oct/Nov 2009) between 50 °N and 40 °S in the upper 150 m in order to investigate the behaviour and distribution of these two essential, bioactive TEs. During *AMT*-19, large differences in the distributions of dCo and dFe were observed. In the North Atlantic gyre provinces, extremely low mixed layer dCo concentrations (23 ± 9 pM) were observed, which contrasts with the relatively high mixed layer dFe concentrations (up to 1.0 nM) coincident with the band of highest atmospheric deposition (~5-30 °N). In the South Atlantic gyre, the opposite trend was observed, with relatively high dCo (55 ± 18 pM) observed throughout the water column, but low dFe concentrations (0.29 ± 0.08 nM). Given that annual dust supply is an order of magnitude greater in the North than the South Atlantic, the dCo distribution was somewhat unexpected. However, the distribution of dCo shows similarities with the distribution of phosphate ($PO_4^{3-}$) in the euphotic zone of the Atlantic Ocean, where the North Atlantic gyre is characterised by chronically low $PO_4$, and higher concentrations are observed in the South Atlantic gyre (Mather et al., 2008), suggesting the potential for a similar biological control of dCo distributions. Inverse correlations between dCo and *Prochlorococcus* abundance in the North Atlantic gyre provinces, combined with extremely low dCo where nitrogen fixation rates were highest (~20-28° N), suggests the

dominance of biological controls on dCo distributions. The contrasting dCo and dFe distributions in the North and South Atlantic gyres provides insights into the differences between the dominant controls on the distribution of these two bioactive trace metals in the central Atlantic Ocean.

## INTRODUCTION

Cobalt (Co), like iron (Fe), is essential for phytoplankton growth (e.g. Morel et al. 1994; Saito et al. 2002; Sunda and Huntsman, 1995a; 1995b; Timmermans et al. 2001; Rodriguez and Ho., 2015). It is required for the de novo synthesis of vitamin $B_{12}$ (cobalamin) by marine prokaryotes (Bonnet et al. 2010), and is the metal co-factor in the metalloenzyme, carbonic anhydrase (CA), which is required for inorganic carbon acquisition by *Prochlorococcus*, and *Synechococcus* (Sunda and Huntsman, 1995a; Saito et al., 2002). In addition, *Trichodesmium* require Co for nitrogen fixation (Rodriguez and Ho, 2015), and Co can substitute for zinc (Zn) as the metal co-factor of the protein PhoA in the enzyme alkaline phosphatase (AP) (Gong et al., 2005; Sunda and Huntsman, 1995a). The production of AP facilitates acquisition of phosphorus (P) from the organic-P pool by phytoplankton and bacteria (e.g. Mahaffey et al., 2014). In addition, the strong correlation between dissolved Co (dCo) and inorganic-P (phosphate,$PO_4$) in the upper water column, across diverse oceanic regimes (Saito and Moffett, 2002; Noble et al., 2008; 2012; Bown et al., 2011; Dulaquais et al., 2014a; Baars and Croot, 2015), indicates the nutritive role of Co.

The role of iron (Fe) as an essential requirement for phytoplankton growth is well documented (e.g. Martin et al., 1990; Coale et al, 1996; Boyd et al., 2007). For example, photosystems I and II are Fe intensive, and Fe is required for enzymatic process at nearly all stages of the microbial nitrogen cycle, including nitrogen fixation (Morel and Price, 2003; Küpper et al., 2008; Richier et al., 2012). Despite Fe being the fourth most abundant element in the Earth's crust, dissolved Fe (dFe) is often only present at trace

concentrations (< 0.5 nM) in oxygenated surface waters of the open ocean (Blain et al., 2008; Measures et al., 2008; Ussher et al., 2013). Consequently, primary production is limited by low Fe-availability in 30 - 40% of the world's oceans (Moore et al, 2002; Boyd and Ellwood, 2010). In the Atlantic Ocean, a number of studies have demonstrated that primary production can be under Fe-stress or limitation, seasonally in association with the spring bloom. (Moore et al., 2006; Nielsdottir et al., 2009), as well as in regions where subsurface nutrient supply is enhanced (Moore et al., 2013, and references therein). The supply of Aeolian Fe is also a key control on the distribution of diazotrophs (Mills et al., 2004; Moore et al., 2009). In addition to Fe, light, macronutrients (N, P, Si), vitamins (e.g. $B_{12}$) and micronutrients (e.g. Co, Zn) may also (co-)limit marine productivity (Bertrand et al., 2007; Saito et al., 2008; Moore et al., 2013; Browning et al., 2014).

A major vector of trace elements (TEs) to Atlantic surface waters is atmospheric deposition (Jickells et al., 2005; Baker et al., 2006; 2007; Sarthou et al., 2007; Buck et al., 2010; Evangelista et al., 2010; Ussher et al., 2013; Shelley et al., 2015), much of which originates from Northwest Africa (Prospero and Carlton, 1972). An estimated 240 ± 80 Tg of dust is transported westwards annually (Kaufman et al., 2005), primarily during the summer months. Approximately 40% of annual global dust deposition occurs in the North Atlantic Ocean (Jickells et al., 2005); the majority of this into waters beneath the Saharan dust plume (~ 5 - 30° N) (Mahowald et al., 1999; Prospero et al., 2002; Kaufman et al., 2005). Hence, it is between these latitudes that surface Fe concentrations are highest (Measures et al., 2008; Fitzsimmons et al., 2013; Ussher et al., 2013). Wet deposition in the Intertropical Convergence Zone (ITCZ) scavenges aerosols from the atmosphere, effectively preventing the southwards transport of North African aerosols (Schlosser et al. (2013). Thus the seasonal migration of the ITCZ drives the latitudinal gradient in aerosol dust loading (Tsamalis et al., 2013; Doherty et al., 2014), and hence surface water Fe concentrations and results in a concomitant shift in the latitudinal distribution of diazotrophy and corresponding dissolved inorganic-P depletion (Schlosser et al., 2013).

Despite Co being less abundant in crustal material than Fe (Fe 3.9%, Co 0.002%; Rudnick and Gao, 2003), atmospheric deposition is a source of Co to surface waters. (Shelley et al., 2012; Dulaquais et al., 2014a). Consequently, we anticipated that Co concentrations would also be highest under the Saharan plume due to the sheer volume of dust that is deposited.

Another important source of trace metals to remote Atlantic surface waters is through vertical mixing. This mechanism reportedly provides ~ 5-35 % of the dFe input flux to the Atlantic mixed layer (Ussher et al., 2013). Vertical mixing is particularly important in the tropics where elevated sub-surface dFe concentrations are associated with low oxygen, upwelled water (Bergquist and Boyle, 2006; Measures et al., 2008; Fitzsimmons et al., 2013; Ussher et al., 2013). On the other hand, lateral advection of Fe from shelf regions to the remote Atlantic Ocean is reported to range from minimal (Laes et al., 2007; Ussher et al., 2007; Noble et al., 2012; Fitzsimmons et al., 2013) to significant in the vicinity of 20 °N (Rijkenberg et al. (2012). For Co, understanding the contribution of these sources is hindered by a relative paucity of data. However, lateral transport has recently been reported in both the eastern and western basins of the Atlantic (Noble et al., 2012; Dulaquais et al., 2014a; 2014b).

Iron and Co distributions are also strongly influenced by both redox speciation and organic complexation. Although $Fe^{2+}$ is the more bioavailable form of Fe (Shaked and Lis, 2012), the thermodynamically favoured species of Fe in oxic seawater (pH 8) is $Fe^{3+}$. However, $Fe^{3+}$ is relatively insoluble under these conditions, and is rapidly scavenged from the water column and forms insoluble $Fe^{3+}$ oxyhydroxides (Liu and Millero, 2002). Chelation by organic ligands increases the solubility of Fe in seawater; both strong (e.g. siderophores) and weaker ligand classes (e.g., humics) have been shown to be play a role in maintaining Fe in solution (Mawji et al., 2008; Croot and Heller, 2012; Heller et al., 2013; Buck et al., 2015). Similarly, $Co^{2+}$ in also thermodynamically favoured in oxic

seawater, and Co forms strong organic complexes (Ellwood and van den Berg, 2001; Saito and Moffett, 2001; Baars and Croot, 2015).

The primary removal mechanism for Co and Fe from the euphotic zone is through biological uptake (Martin and Gordon, 1988; Moffett and Ho, 1996). In addition, adsorptive scavenging on to particles (Moffett and Ho, 1996; Johnson et al., 1997; Wu et al., 2001; Bruland and Lohan, 2003) and aggregation and sinking (Croot et al., 2004) are also important removal pathways for both Co and Fe.

The Atlantic Meridional Transect (*AMT*) programme provides an ideal platform to investigate Co and Fe cycling in the upper Atlantic Ocean and the role of these metals on climate-relevant biological processes. Here we report the geographical distribution and biogeochemistry of Co and Fe in the upper water column along a 12,000 km, gyre-centred transect of the Atlantic Ocean (*AMT-19*) between ~ 50° N and 40° S. As our knowledge of Fe biogeochemistry is arguably more advanced than for Co, the following discussion aims to develop our understanding of Co biogeochemistry in the upper water column (≤ 150 m) of the Atlantic Ocean between 50° N and 40 °S by making comparisons with dissolved Fe distributions from this and earlier studies.

## MATERIALS AND METHODS

### *Sampling*

Twenty nine stations were sampled during cruise *AMT-19* (13/10/09–28/11/09) from Falmouth, UK to Punta Arenas, Chile, on board the *R.R.S. James Cook* (Fig. 1). Stations were sampled from the six biogeographical provinces listed in Figure 1, described by Longhurst (1998). In this study, the distribution of salinity, temperature, dCo, dFe and macronutrients (nitrate and phosphate) were used to identify the province boundaries (Table 1). The assigned province boundaries are subject to small-scale variations due to their seasonal drift, as is the ITCZ, a region that forms the boundary between the atmospheric

135 hemispheres which migrates seasonally from a position centred at ~5°N in boreal winter to
136 ~10°N in the boreal summer (Sultan and Janicot, 2000).

137

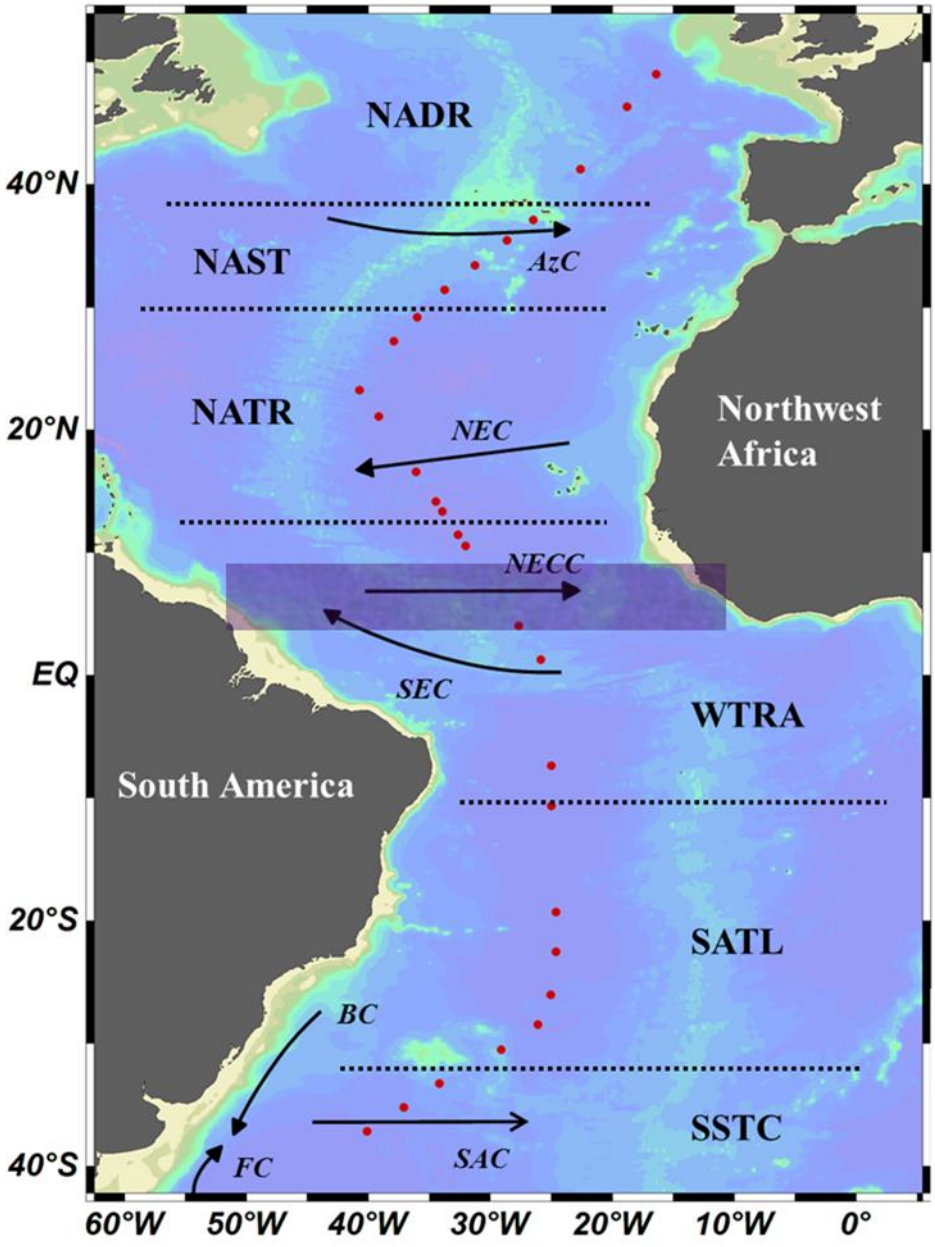


138

139 Figure 1. AMT-19 cruise track, showing the 29 water column stations and the biogeochemical
140 provinces (Longhurst, 1998) defined in this study: North Atlantic Drift (NADR,38-56°N), North Atlantic
141 Gyre (NAST,30-38°N), North Atlantic Tropical Gyre (NATR,12-30°N), Western Tropical Atlantic
142 (WTRA,12°N-10°S), South Atlantic Gyre (SATL,10-33°S), and South Atlantic Subtropical
143 Convergence (SSTC, 33-55°S), and Atlantic Ocean surface currents: AzC = Azores Current, NEC =

North Equatorial Current, NECC = North Atlantic Counter Current, SEC = South Equatorial Current, BC = Brazil Current, SAC = South Atlantic Current, FC = Falklands Current. The approximate position of the ITCZ (4-9°N with the most intense rain activity between 4-5°N) during November 2009 was identified from the Giovanni data product (http://giovanni.sci.gsfc.nasa.gov), and is marked by the shaded box.

Samples for the determination of dCo and dFe were collected from 10 L trace metal-clean Teflon coated Ocean Test Equipment (OTE) bottles, attached to a titanium CTD rosette. Samples for macronutrients were collected from ten depths during each titanium CTD rosette deployment to correspond with trace metal sampling, and additionally from standard 20 L Niskin bottles fitted to a stainless steel CTD rosette (Seabird), thus providing high resolution profiling along the cruise track. All ship-based trace metal sample handling was conducted in a pressurised clean van. Seawater samples for dCo and dFe were filtered into acid-cleaned, low density polyethylene (LDPE) bottles (Nalgene) using a 0.2 µm Sartobran 300 filter capsule (Sartorius) and acidified to pH 1.7-1.8 (0.024 M) with ultraclean hydrochloric acid (HCl, Romil SpA) inside a class-100 laminar flow hood. Samples for the determination of TdFe were not filtered prior to acidification to 0.024 M HCl. All samples were then double zip-lock bagged for storage prior to analysis in the home laboratory.

*Dissolved cobalt determination*

Dissolved Co was determined in the ISO accredited clean room facility (ISO 9001) at Plymouth University, UK by flow injection with chemiluminescence detection (FI-CL; Shelley et al., 2010). Briefly, the flow injection manifold was coupled with a photomultiplier tube (Hamamatsu, model H 6240-01). The dCo was determined in UV-irradiated samples (3 h; 400 W medium-pressure Hg lamp, Photochemical Reactors) from the chemiluminescence produced from the catalytic oxidation of pyrogallol (1,2,3-trihydroxybenzene), the chemiluminescence emission was recorded using LabVIEW v.7.1 software. Due to the extremely stable nature of organic complexes of Co in seawater, several studies have

demonstrated the requirement to UV irradiate samples prior to analysis in order to liberate strongly-complexed Co (Vega and van den Berg, 1997; Donat and Bruland, 1988; Saito et al., 2005; Shelley et al., 2010). During all analytical runs UV-irradiated SAFe D2 reference samples were analysed ($n$ = 4; measured value, 50 ± 2 pM; consensus value 46± 3 pM). Typically, blank values were 4 ± 1 pM ($n$ = 8), with a detection limit of 3 pM (blank + 3σ).

*Dissolved and total dissolvable iron determination*

Dissolved Fe and total dissolvable Fe (TdFe; unfiltered seawater) were also determined using FI-CL in the same clean room facility as the dCo. The Fe FI-CL method used in this study was based on the method originally described by Obata et al. (1993) and modified by de Baar et al. (2008). Briefly, measurements were made based on the catalytic oxidation of luminol (5-amino-2,3-dihydrophthalazine-1,4-dione; Aldrich) by hydrogen peroxide ($H_2O_2$) in the presence of Fe. As this method detects Fe(III), this study used a $H_2O_2$ oxidation step whereby $H_2O_2$ (10 nM) was added to each sample 1 h prior to the determination of Fe(III) (Lohan et al., 2005). Chemiluminescence emission was detected by a Hamamatsu photomultiplier tube (model H 6240-01) and recorded using LabVIEW v.7.1 software. The accuracy of the method was assessed for every analytical run by the determination of dFe in SAFe S and D1 seawater reference materials. The concentrations of dFe measured in the SAFe reference samples were in good agreement with the consensus values (measured value, $S$ = 0.12 ± 0.04 nM, $n$ = 13; D1 = 0.72 ± 0.08 $n$ = 14; consensus value, $S$ = 0.093 ± 0.008 nM; D1 = 0.67 ± 0.04).

Consensus values for dCo and dFe were reported to the GEOTRACES Intercalibration Committee in 2010 (dCo) and 2011 (dFe), and are available at:http://geotraces.org/science/intercalibration/322-standards-and-reference-materials.

*Nutrients, temperature, salinity and chlorophyll-a*

Dissolved inorganic macronutrients, phosphate ($PO_4^{3-}$) and nitrate ($NO_2^- + NO_3^- = \Sigma NO_3$) were analysed on-board within 3-4 h of collection using a 5-channel segmented flow autoanalyser (Bran and Luebbe, AAII AutoAnalyzer) following standard colorimetric procedures (Grashoff et al. 1983) modified by Woodward et al. (1999). Low-level nutrients were not determined using liquid wave guides during *AMT*-19.

Salinity, temperature and dissolved $O_2$ were measured using a CTD system (Seabird 911+). Dissolved $O_2$ was determined by a Seabird SBE 43 $O_2$ sensor. Salinity was calibrated on-board using discrete samples taken from the OTE bottles using an Autosal 8400B salinometer (Guildline), whilst dissolved $O_2$ was calibrated using an automated photometric Winkler titration system (Carritt and Carpenter, 1966). Chlorophyll fluorescence and beam attenuation were determined using an Aquatraka MkIII fluorometer and Alphatraka MkII transmissometer (Chelsea Instruments), respectively. Sampling depths were determined by reference to the *in situ* fluorescence, temperature, salinity and irradiance (photosynthetically active radiation, PAR, 400–700 nm) profiles, to include 97%, 55%, 33%, 14%, 1% and 0.1% PAR levels. For chlorophyll-*a* determination, samples were filtered (0.2 µm polycarbonate) and the filters extracted in 10 mL of 90 % acetone overnight at 4° C (Welschmeyer et al., 1994). The chlorophyll-*a* extract was measured on a pre-calibrated (pure chlorophyll-*a* standard, Sigma-Aldrich) Turner Designs Trilogy 700 fluorimeter.

*Prochlorococcus* and *Synechococcus* were enumerated by flow cytometry using a Becton Dickinson FACSort (Oxford, UK) flow cytometer equipped with an air-cooled laser providing blue light at 488 nm (Tarran et al. 2006).

The trace metal (dCo, dFe and TdFe) data, ancillary data and a full station list are available at: http://www.bodc.ac. uk/ projects/uk/amt/

## RESULTS

### *Hydrographic setting and macronutrient distributions*

The six biogeographical provinces used in this study are shown in Figure 1. Note that the North Atlantic gyre is divided into two separate provinces; the North Atlantic subtropical gyre (NAST) and the North Atlantic tropical gyre (NATR). In these provinces, the thermohaline structure of the upper water column (Fig. 2) is primarily determined by the water masses that occupy each region and the relative evaporation and precipitation rates. In the North Atlantic, the lowest upper water column temperatures (12-22°C) were observed in the NADR. Here, the water column displayed weak thermohaline stratification, characteristic of high wind stress in the NADR during boreal autumn (Longhurst, 1998).

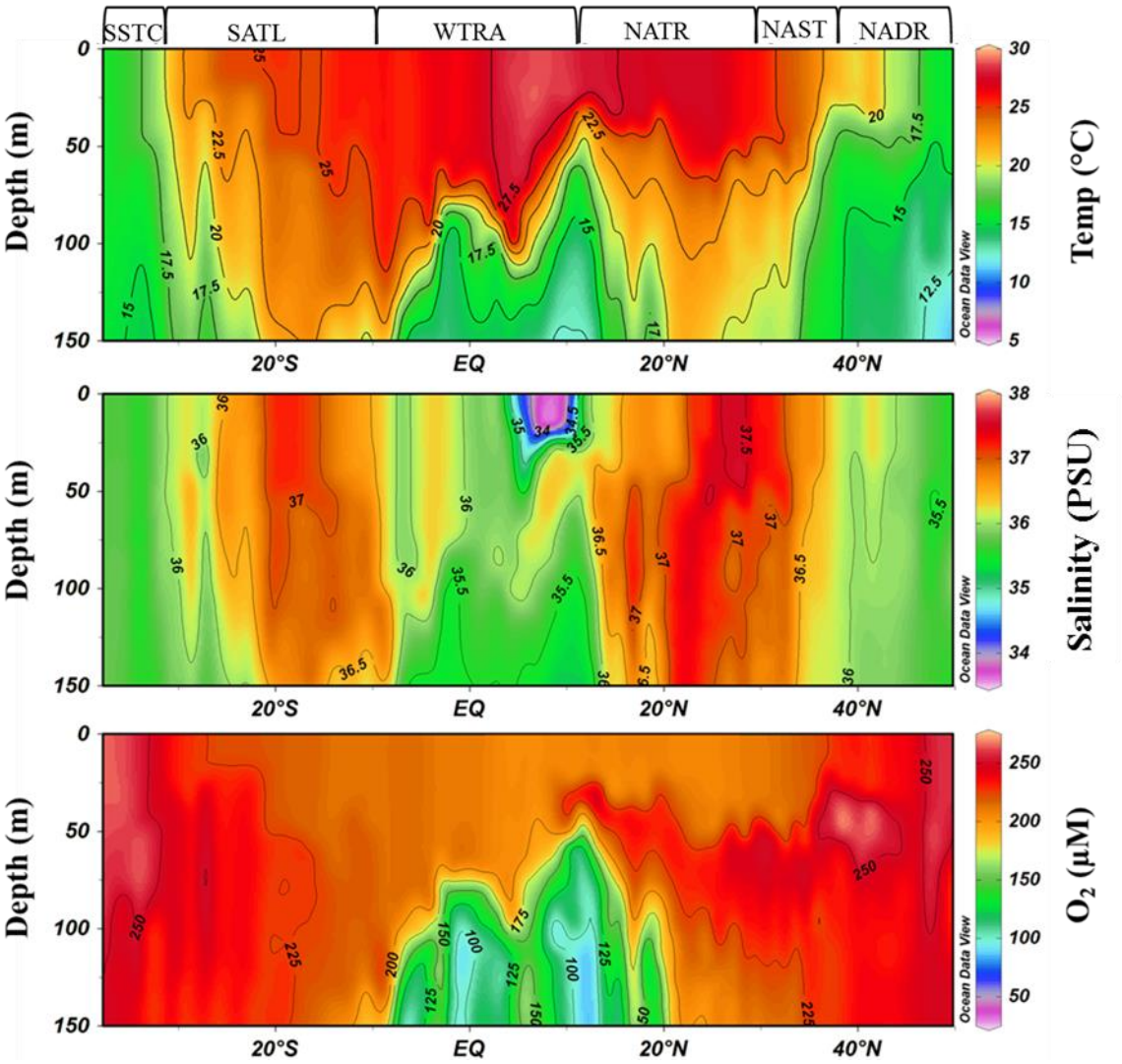


Figure 2. The distributions of temperature (top), salinity (middle) and dissolved oxygen (bottom) in the upper 150 m of the Atlantic Ocean during *AMT*-19, with the biogeochemical provinces marked above (refer to Figure 1 for acronyms). Stations were sampled approximately every 1-1.5° of latitude at a 1 m depth resolution.

In the NAST, the introduction of warmer (> 20° C), more saline (> 36.5), water from the Gulf Stream enters via the Azores Current (AC, centred at 35-36 °N) (Aiken et al., 2000) resulting in a mixed layer depth of between 40 and 50 m. Further south in the NATR, the North Equatorial Current (NEC, centred at 15 °N) supplies water with salinity > 37, due to the high rates of evaporation at these latitudes. Consistent with previous *AMT* observations (Aiken et al., 2000; Robinson et al., 2006), the NEC was observed to depths of ~ 150 m between 20 and 26° N during *AMT*-19.

Towards the southern extent of the NATR province, a plume of cooler (< 20° C), fresher (< 36), lower oxygen (< 150 µM) upwelled water was clearly visible below 60 m (Fig. 2). This oxygen minimum zone (OMZ), which extended throughout the tropical Atlantic to the southern boundary of the WTRA, results from the divergence between the North Equatorial Current (NEC) and the North Equatorial Counter Current (NECC) at ~ 10° N, and the divergence between the NECC and the South Equatorial Current (SEC) at ~ 2° S (Hastenrath and Merle, 1987; Longhurst, 1998; Aiken et al., 2000) (Fig. 1). Mixed layer depths (defined as the depth at which potential density differed by 0.05 kg $m^{-3}$ from the surface) in the WTRA varied between 9 and 95 m. Throughout the upper 150 m of the WTRA low salinity (< 36.5) water, relative to the sub-tropical gyres, was observed caused by dilution through excess precipitation over evaporation (Aiken et al., 2000).

A surface salinity minimum (< 35) was observed in the WTRA between ~6 and 10° N to a depth of 30 m (Fig. 2), a common feature that can arise from either converging air masses and subsequent high precipitation rates in the ITCZ, or from Amazon Water transported eastwards across the Atlantic by the NECC (Aiken et al., 2000). However, no elevation in surface silicate concentration (data not shown), which would be indicative of Amazon Water, was observed during *AMT*-19. In addition, two intense rainfall events were

recorded between 6 and 9 °N during the cruise, suggesting that the high rates of precipitation that characterise the ITCZ could be the cause of the WTRA salinity minimum.

As observed during earlier *AMT* studies (Robinson et al., 2006), a gradual latitudinal decrease in sea surface temperature and salinity was observed in the SATL (10-33° S) and into the SSTC (33 -38° S), a manifestation of the decrease in evaporation rates associated with lower temperatures at higher latitudes. An increase in the westerly winds as the ship travelled south, coupled with increased downwelling associated with the anti-cyclonic circulation of the sub-tropical gyre (Longhurst, 1998; Ussher et al., 2013), resulted in a deepening of the SATL mixed surface layer down to 61 m, and a fully homogeneous upper water column ($T$ ~ 16 °C, $S$ ~ 35.5) in the SSTC.

The distribution of macronutrients along the transect (Fig. 3; $NO_3$ data is not shown due to the similarity with the distribution of $PO_4$) revealed extremely low mixed layer concentrations ($PO_4$ < 0.05 µM) in the NAST and NATR and three distinct regions where concentrations below the mixed layer were elevated. Firstly, in the NADR, macronutrient concentrations were elevated below 60 m ($PO_4$ = 0.2-0.9 µM, $NO_3$ = 2.5-12 µM). These elevated concentrations continued into the northern section of the NAST before becoming depleted. Secondly, macronutrient concentrations were elevated in waters associated with the equatorial upwelling ($PO_4$ =0.2-1.5 µM, $NO_3$ = 2.5- 23 µM). Thirdly, macronutrient concentrations in the SSTC were elevated below 100 m ($PO_4$ = 0.2- 0.5 µM; $NO_3$ = 2.5- 5 µM), values similar to those reported for the Southwest Atlantic at 40° S by Wyatt et al. (2014).

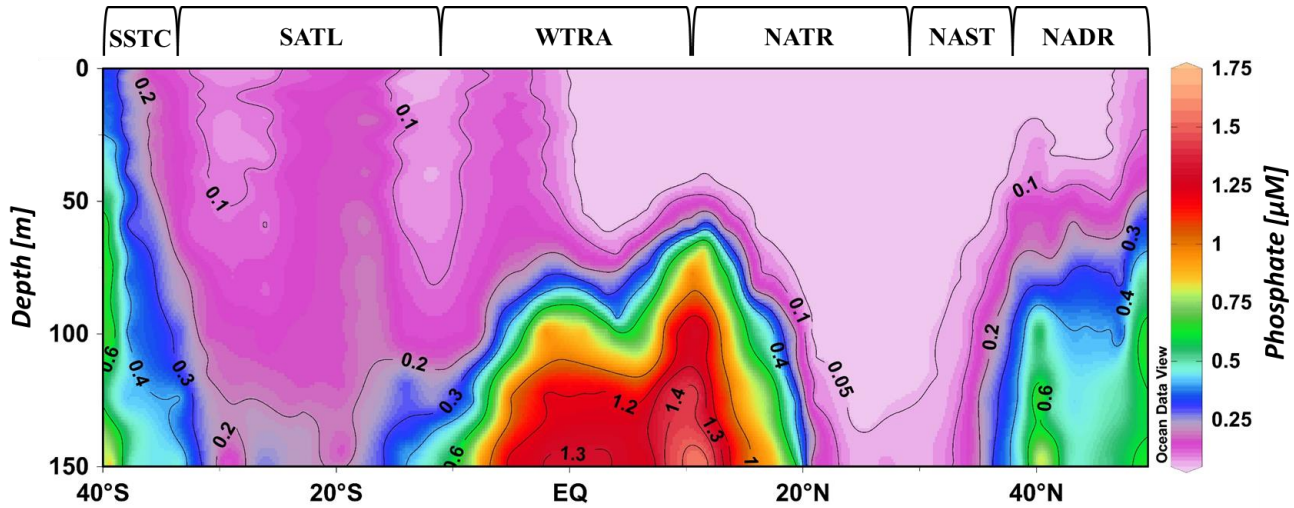


Figure 3. Distribution of phosphate ($PO_4$) in the upper 150 m of the Atlantic Ocean during *AMT* 19 with the biogeochemical provinces marked above (refer to Figure 1 for acronyms). Note the higher concentrations in the SATL compared to the NAST and NATR.

Dissolved Co and Fe distributions

Surface water (upper 25 m) dCo and dFe distributions during *AMT*-19 displayed distinct differences between the North and South Atlantic (Fig. 4). Surface dCo concentrations during *AMT*-19 were highly variable (10-93 pM). The lowest concentrations were observed in the northern gyre provinces (NAST 25 ± 14 pM and NATR 21 ± 2.8 pM, respectively, n = 6), whilst higher concentrations were observed in the upwelling region (WTRA 51 ± 38 pM, n = 9) and the South Atlantic gyre (SATL 60 ± 31 pM, n = 3) (Fig. 4) This trend is similar to that previously reported for $PO_4$, with very low concentrations of $PO_4$ (0.01-0.05 µM) observed in the North Atlantic gyre regions and higher concentrations (0.2-0.5 µM) in the South Atlantic gyre (Mather *et al.,* 2008). At approximately 28° S the SATL is sub-divided into two cells separated by the subtropical counter-current. To the south of this front (25-30° S) the Brazil Current (BC) forms the southern extent of a recirculation cell (Mémery et al. 2000 and references therein). The high surface dCo in this region (89 ± 4 pM at 28.8°S, 26.1°W, Fig. 4) is attributed to offshore advection of continental Co mobilised by the western boundary current and a declining gradient is observed to the south of this frontal region.

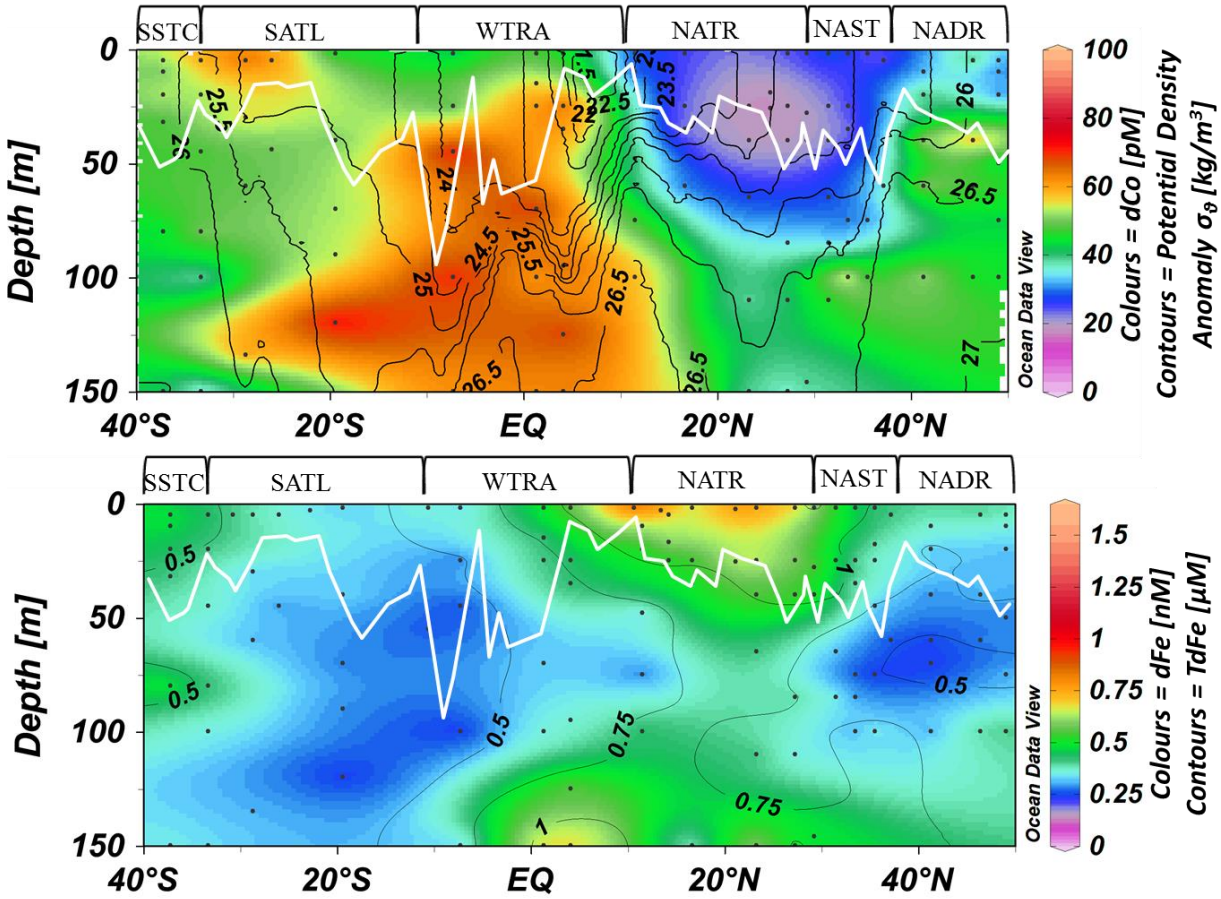


Figure 4. The distribution of dCo (pM) overlaid with potential density anomaly (kg $m^{-3}$; top panel), dFe (nM) overlaid with the TdFe (nM; bottom panel) in the upper 150 m of the Atlantic Ocean during *AMT*-19, with the approximate depth of the mixed layer marked (MLD) shown as a solid white line. The biogeochemical provinces are displayed above the top panel (refer to Figure 1 for acronyms).

The surface water (upper 25 m) dFe and TdFe distribution is in complete contrast to dCo, as dFe and TdFe were relatively high in the NATR and NAST, and low in the SATL (Fig. 4). The highest surface dFe and TdFe concentrations were observed in the NATR (dFe, 0.68 ± 0.28 nM; TdFe, 1.1 ± 0.25 nM, n = 12 and 10, respectively) and the WTRA (dFe, 0.76 ± 0.61 nM; TdFe 1.3 ± 0.33 nM, n = 6) provinces between ~ 5 and 30° N, corresponding to the latitudinal extent of the Saharan plume (5-30° N) (Prospero et al. 2002; Kaufman et al., 2005). Here, two distinct surface dFe maxima were observed. The first, located between ~ 20 and 28° N (dFe, 0.88 ± 0.14 nM, n = 6), was in the vicinity of the elevated rates of surface nitrogen fixation (0.85-1.1 nmol $L^{-1}$ $d^{-1}$) determined during this study (data not shown, but available from www.bodc.ac.uk). The second, at ~10-14° N (0.74 ± 0.58 nM, n = 7),

316 overlapped with the ITCZ surface salinity minimum (Fig. 2), which is consistent with the
317 observation that high rainfall rates associated with the ITCZ contributes to high wet
318 deposition fluxes of Fe in the south NATR/north WTRA (Kim and Church, 2002; Powell et al.,
319 2015). The locations of these two surface dFe maxima coincided with high TdFe
320 concentrations (1.1 ± 0.17 nM and 1.3 ± 0.28 nM, respectively) between 4 – 30° N, and are
321 in excellent agreement with observations from previous North Atlantic studies (Bowie et al.,
322 2002; Bergquist and Boyle, 2006; Measures et al., 2008; Ussher et al., 2013). Combined
323 with the low dFe in the SATL, the peaks in dFe and TdFe in the North Atlantic gyre provinces
324 indicate the importance of atmospheric deposition in controlling surface dFe concentrations
325 (e.g., Schlosser et al. 2013). North of ~ 30° N, surface dFe concentrations were lower (0.34
326 ± 0.14 nM, n = 14) and less variable (Fig. 4), most likely due to a reduced Saharan dust
327 input and strong winter mixing in the NAST and NADR, compared with weak seasonal
328 mixing in the NATR (Longhurst, 1998).

329 In sub-surface waters (deeper than 25 m), the dCo distribution was also a tale of
330 sharp contrasts. Extremely low concentrations were observed throughout the North Atlantic
331 gyre provinces, with the lowest concentrations (16 ± 3.4 pM, n = 8) observed at the base of
332 the mixed layer. The maximum abundances of *Prochlorococcus* (> 4 x $10^5$ cells $mL^{-1}$), a
333 cyanobacteria with an absolute requirement for Co (Sunda and Huntsman, 1995a), in the
334 North Atlantic gyre provinces were observed in the southern NATR in concert with a shoaling
335 of the MLD, and were accompanied by very low dCo concentrations (13-17 pM at 35-40 m
336 depth), suggesting biological drawdown as an important control of dCo distribution in this
337 region. Higher dCo concentrations were observed in the provinces adjoining the northern
338 gyre provinces, e.g., in the NADR (dCo = 59 ± 23 pM, n = 10) *Prochlorococcus* were less
339 abundant and dCo appears to be advected southwards along the 26 kg $m^{-3}$ isopycnal (Fig. 4,
340 top panel) to ~ 40°N and the boundary with the NAST.

341 The highest sub-surface dCo concentrations (e.g. 89 ± 4 pM at 28.8°S, 26.1°W) were
342 observed in the SATL. Between 25-150 m, the SATL was characterised by relatively high

dCo (52 ± 15 pM, n = 10), and decreasing temperature and salinity with increasing latitude. At the dynamic SATL/SSTC boundary (33.3°S, 34.2°W), a slight increase in dCo was observed at 80 m relative to the surrounding water (58 pM at 80 m, 44 pM at 45 m and 29 pM at 100 m). The source of this high dCo is not immediately clear, but may result from spin-off of eddies containing higher dCo water from the south. The presence of eddies in this region is confirmed by the sea surface anomaly image, Fig. S1 in the Supplementary Material. As concentrations of dCo can be highly variable over scales of ~10 km (Saito and Moffett, 2002; Noble et al. 2008; Shelley et al. 2012), the low dCo observed at the adjoining station (15.5 ± 0.3 pM at 35.3°S, 37.1°W) may be just as characteristic of this province (reflecting seawater that has had no contact with the continental shelf and low atmospheric inputs) as water with high dCo. Regardless of the dCo concentration, in all gyre provinces dCo exhibited a broadly nutrient-type distribution (lower concentrations in the mixed layer than below it) in the upper 150 m.

The sub-surface distribution of dFe also displayed strong latitudinal gradients (Fig. 4.) In a reversal of the trend for dCo, sub-surface dFe concentrations in the SATL were low and relatively uniform (0.26 ± 0.06 nM, n = 12) compared with the northern gyre provinces (0.40 ± 0.17 nM, n = 25) where atmospheric deposition is much higher. Below 100 m in the northern NATR/southern NAST waters between 23 and 31° N, the dFe andTdFe concentrations were 0.48 ± 0.14 nM (n = 5) and 0.72 ± 0.11 nM (n = 5), respectively and could be a relic of a previous atmospheric deposition event. Interestingly, we observed a similar feature at the same depth for dCo (36 ± 3.4 pM; Fig. 4).

For both dCo and dFe, elevated sub-surface concentrations were associated with the low oxygen waters. Maximum sub-surface dCo and dFe concentrations (62 ± 16 pM and 0.62 ± 0.20 nM, respectively) were observed between 0-10 °N, coincident with an oxygen minimum of 100 -150 µM (Fig. 2). Observations of elevated dFe in this OMZ are consistent with previous studies (Bergquist and Boyle, 2006; Measures et al., 2008; Fitzsimmons et al., 2013; Ussher et al., 2013) suggesting that the elevated dFe may be a steady-state feature in

this region, sustained by either remineralisation of high Fe:C organic matter formed in the Fe-rich surface and/or lateral mixing of high dFe water from sedimentary sources. However, in contrast to dFe, the elevated dCo concentrations were not confined to the OMZ, but extended over a broader latitudinal range (southwards) and wider depth range, suggesting that mechanisms other than remineralisation and low dissolved oxygen concentrations were sustaining the elevated dCo concentrations in this region.

## DISCUSSION

Given that there are a number of similarities in the redox and organic speciation of Co and Fe, the difference in the distributions of these two elements in the Atlantic Ocean is stark. In the northern gyre provinces (NATR and NAST), where deposition and dissolution of atmospheric aerosols is the dominant source of Fe (e.g. Duce and Tindale, 1991; Duce et al. 1991; Sarthou et al., 2003; Jickells et al., 2005; Baker et al., 2006; Buck et al., 2010; Evangelista et al., 2010; Ussher et al., 2013), the extremely low concentrations of dCo contrast strongly with the relatively high concentrations of dFe. A number of studies have alluded to an atmospheric source of Co which could influence surface dCo concentrations in regions of high atmospheric deposition (Bowie et al. 2002; Dulaquais et al., 2014a; Knauer et al, 1982; Thuroczy et al., 2010; Wong et al. 1995). Furthermore, aerosol Co is significantly more soluble than aerosol Fe (Dulaquais et al., 2014a; Mackey et al., 2015; e.g. 8-10% fractional solubility for Co and 0.44-1.1% fractional solubility for Fe for the same Saharan dust samples, Shelley et al., 2012), further supporting the assertion that atmospheric supply may play a pivotal role in controlling surface distributions of dCo and hence influence phytoplankton community dynamics.

For dFe, the sharpest gradient was observed at the NAST/NATR boundary, and is almost certainly linked to atmospheric inputs and the approximate location of the northern extent of the Saharan plume. Indeed the relationship between dFe in the upper water

column and atmospheric supply are well documented (e.g. Bowie et al., 2002; Baker et al. 2006, 2007; 2013; Rijkenberg et al., 2012; Ussher et al., 2013), which makes the low dCo in the same latitudinal band somewhat of a paradox. One explanation could be that the Co is being scavenged in the water column following oxidation by manganese (Mn) oxidising bacteria, which oxidise both Mn and Co via a common microbial pathway (Moffet and Ho, 2001). However, significant removal via the Mn co-oxidation pathway is not supported by the literature in open ocean environments, as it is driven by competitive inhibition (Moffett and Ho, 1996; Noble et al., 2012) and dCo is low (this study; A. Noble, pers. comm.) and Mn is high (Wu et al., 2014; Hatta et al., 2015) in the northern gyre provinces.

In the vicinity of the ITCZ, both dFe and TdFe were significantly inversely related to salinity in the mixed layer ($r^2$ = 0.89 and 0.82 respectively; $p < 0.05$, n = 5) suggesting that the scavenging of dust incursions into the ITCZ as it migrated south towards to its boreal winter position (centred at ~ 5° N) could be a source of Fe to surface waters at the NATR/WTRA border, as described by Kim and Church (2002). However, the small number of samples (n = 5) make any links tenuous at best, particularly as this relationship is driven by the high dFe and TdFe values (both 1.1 nM) at 1.5 m depth at 10.6 °N, 32.0 °W). Similarly, the relatively sparse dCo dataset for mixed layer waters influenced by the ITCZ (n = 4) makes assessing a link between dCo and precipitation unrealistic, and is further complicated by the limited literature on dCo in rainwater of the ITCZ and the contrasting conclusions reached; i.e. either precipitation dilutes surface dCo (Helmer and Schremms, 1995; Pohl et al., 2010), or it is a source of dCo (Bowie et al., 2002). In this study, two modest enrichments of dCo (relative to the underlying water and to adjoining stations) coincided with rain events at 31 °N, and the intense rain events in the ITCZ at 6 and 9 °N (M. Chieze, pers. comm). At 31 °N, for example, the concentration of dCo was 46.4 pM at 2 m depth, whereas at 25 m depth dCo had been drawn down to 21.2 pM. In addition, wet deposition has been estimated to account for >90% of the total atmospheric deposition flux of Co, compared with just 20% for Fe, based on data from Bermuda (T. Church, unpublished

423 data). In the eastern tropical Atlantic (in September-November), Powell et al. (2015) estimate
424 that wet deposition may be a relatively more important source of Fe than in the western
425 North Atlantic gyre, contributing up to 70% of the total atmospheric flux.

426 We have estimated the soluble Co and Fe deposition fluxes for 20 °N and 20 °S from
427 dry deposition data published in Shelley et al. (2015) and Dulaquais et al. (2014a) (20 °N)
428 and Chance et al. (2015) (20 °S) (Table 1). For Co, in the NATR, under the Saharan outflow,
429 dry deposition contributes only 1.4% of the mixed layer depth (MLD) concentration of dCo
430 (assuming permanent stratification of the water column). In contrast, atmospheric deposition
431 may supply twice the amount of dFe observed in the mixed layer over the course of the year.
432 In the SATL, where atmospheric deposition may be orders of magnitude lower, atmospheric
433 supply alone cannot account for the concentrations of either metal observed (<<0.5% and
434 21% of mixed layer dCo and dFe, respectively). It is noted that these atmospheric deposition
435 fluxes do not account for wet deposition, and thus, the estimates presented in Table 1 may
436 be rather conservative. Nonetheless, these data highlight the role of atmospheric deposition
437 in controlling the dFe concentrations in surface waters of the two gyre regions. For Co, the
438 impact of atmospheric deposition is more subtle.

439 Our calculations are sensitive to the percentage of the metal that is soluble in
440 seawater. Unfortunately, aerosol metal solubility is poorly constrained. In Table 1, a Co
441 solubility value of 9.0% is used for the NATR (Dulaquais et al., 2014a). However, Co
442 solubility is a function of the composition of the bulk aerosol, which in turn is a function of
443 aerosol provenance, and may be up to threefold higher (i.e., ~30%, R. Shelley, unpublished
444 data, available at: www.bco-dmo.org) in aerosols sourced from Europe as opposed to those
445 from North Africa, due to a higher component of industrial emission aerosols in the former.
446 This will result in a higher flux of soluble Co, and given the extremely low concentrations of
447 dCo in the northern gyre provinces, suggests that atmospheric supply may still have an
448 important role in supplying Co to surface waters (Thuroczy et al., 2010).

Table 1. Estimation of the contribution of atmospheric dry deposition to the mixed layer (ML) inventories of dCo and dFe. The values used are from: a = Shelley et al. (2015); b = Dulaquais et al., 2014a; c= this study; d = Chance et al. (2015), respectively.

| Metal | Location | Dry depo. flux | Solubility | Soluble flux | | MLD | MLD [dCo, dFe] | Annual accumulation in ML |
|---|---|---|---|---|---|---|---|---|
| | | μg $m^{-2}$ $d^{-1}$ | % | μg $m^{-2}$ $d^{-1}$ | nM $m^{-2}$ $d^{-1}$ | m | nM | nM |
| Cobalt | 20 N | 1.6 (a) | 9.0 (b) | 0.14 (a, b) | 24 (a, b) | 40 (c) | 16.2 (c) | 0.22 |
| Cobalt | ~ 20 S | 0.0029 (d) | 2.0 (d) | 0.000058 (d) | 0.010 (d) | 45 (b) | 37 (b) | 0.000080 |
| Iron | 20 N | 3600 (a) | 0.31 (a) | 11.2 (a) | 201 (a) | 40 (c) | 0.90 (c) | 1.80 |
| Iron | ~ 20 S | 3.2 (d) | 2.9 (d) | 0.093 (d) | 1.7 (d) | 45 (c) | 0.33 (c) | 0.014 |

If, as our data suggests, aerosols are indeed a source of Co to the northern gyre provinces, how can the contrasting distributions of dCo and dFe be reconciled? We hypothesise that biological uptake primarily by the cyanobacteria, principally *Prochlorococcus* and *Trichodesmium,* is exceeding supply, leading to a dCo deficit in the northern gyre provinces (NAST, NATR).

*Biological controls on dissolved Co distributions*

Although *Prochlorococcus* are ubiquitous in tropical and sub-tropical oceans, their range extends throughout the Atlantic from ~50 °N – 40 °S (Heywood et al., 2006). *Prochlorococcus* thrive in oligotrophic conditions and have an obligate requirement for Co for carbon fixation (Sunda and Huntsman, 1995a; Saito et al., 2002). During *AMT*-19, *Prochlorococcus* dominated the picoplankton assemblage, with *Synechococcus* only proliferating where *Prochlorococcus* abundance was less than $10^5$ cells $mL^{-1}$ (Fig. 5), i.e., the temperate margins of this *AMT* transect (NADR and SSTC), and in the low-salinity (<35) surface waters of the ITCZ (upper 30 m at 6-10 °N; Fig.2). Our data are consistent with the observation that *Prochlorococcus* typically outnumber *Synechococcus* by one to two orders of magnitude in stratified, oligotrophic waters (Durand et al., 2001).

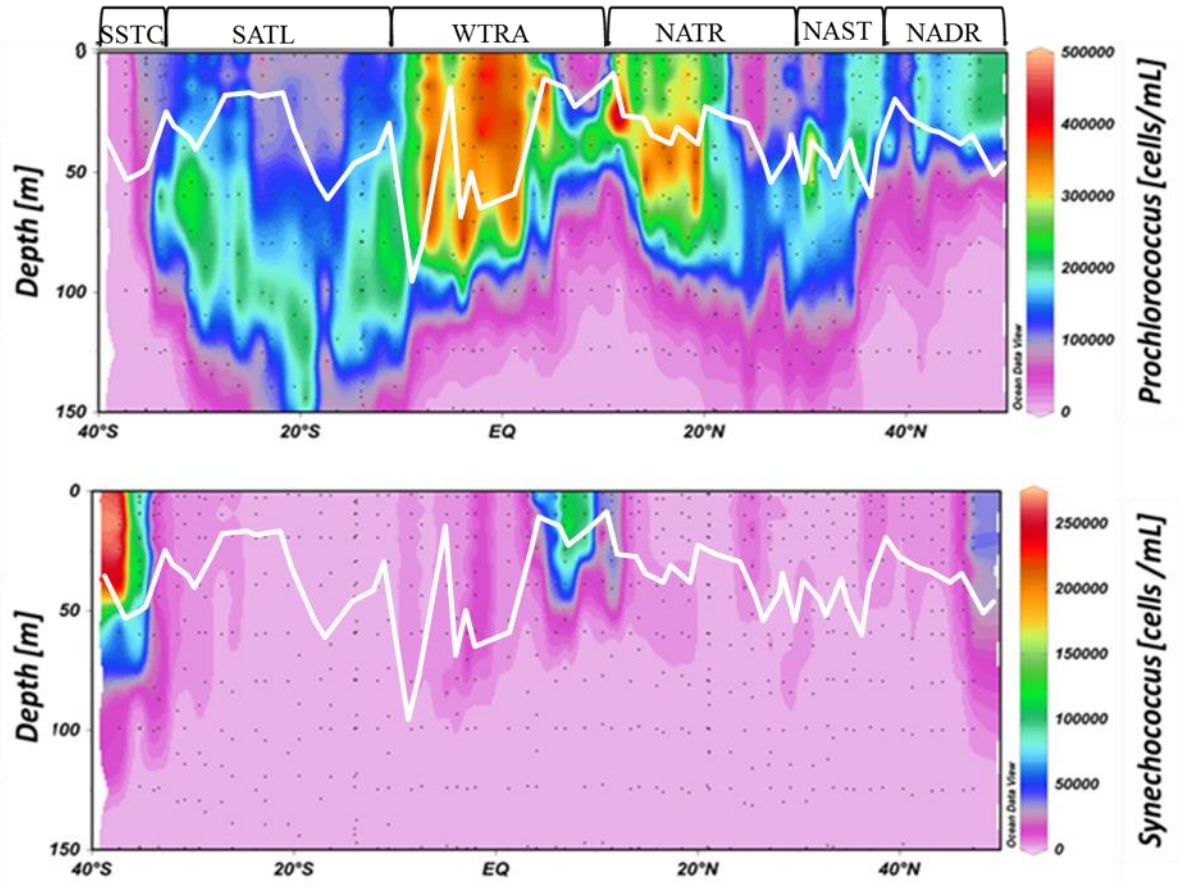


Figure 5. *Prochlorococcus* and *Synechococcus* distributions in the upper 150 m during *AMT*-19. The white line depicts the approximate depth of the mixed layer.

In this study, the highest abundances of *Prochlorococcus* were observed in the high-dCo tropical upwelling region (~5 °N-5 °S) (Fig. 5). This contrasts with the phytoplankton dynamics in another high dCo upwelling region, the Costa Rica upwelling dome (CRD), where *Synechococcus* dominated the picoplankton assemblage (Ahlgren et al., 2014).

In terms of *Prochlorococcus* abundance, the northern gyre was divided in two (at approximately the boundary between the NATR and NAST). The NAST and NATR, were both characterised by extremely low dCo concentrations, with the dCo minima (NAST = 15 ± 3.8, NATR = 15 ± 1.4 pM, at 28-45 m) generally corresponding with the maximum abundances of *Prochlorococcus* in these provinces (Fig. 5). The *Prochlorococcus* maxima were at shallower depths than the DCM (e.g., 4 x$10^5$ cells $mL^{-1}$ at 29 m at 11.5 °N, compared to a DCM of 0.41 µg $L^{-1}$ chl-*a* between 46-50 m ). The relationship between dCo

484 distributions, *Prochlorococcus* abundance, and the relative position of the DCM has
485 previously been observed in the Sargasso Sea (western NAST/NATR; Shelley et al., 2012).

486 In the NATR, *Prochlorococcus* abundance was high (>3x10$^5$ cells mL$^{-1}$), even though
487 dCo was extremely low (22 ± 15 pM). In the NAST, dCo was similarly low (22 ± 3.8 pM), but
488 *Prochlorococcus* abundance was lower than in the NATR (generally <2x10$^5$ cells mL$^{-1}$). As
489 atmospheric deposition decreases northwards from the NATR to NAST, we hypothesise that
490 aerosol supply indirectly impacts *Prochlorococcus* abundance via its role as a key source of
491 Co and Fe. Moreover, the sub-surface dCo minimum coincides with the region of maximum
492 rates of nitrogen fixation during *AMT*-19 (21 – 23°N), consistent with a Co requirement for
493 nitrogen fixation by *Trichodesmium* (Rodriguez and Ho, 2015), which are abundant in the
494 tropical to subtropical North Atlantic, but almost entirely absent between 5 and 30° S (Tyrrell
495 et al., 2003; Schlosser et al., 2013). In the SATL, dCo concentrations and *Prochlorococcus*
496 abundance were decoupled to the extent that the opposite trend was observed, with high
497 dCo and high abundances of *Prochlorococcus* occurring together. This occurred in concert
498 with a near absence of *Trichodesmium*, suggesting that the presence/absence of
499 *Trichodesmium* may also have an important role in driving the dCo distribution. Furthermore,
500 the contrasting dCo distributions cannot be explained by other components of the bacterio-
501 plankton assemblage as bacterial abundance was roughly equivalent in the SATL and
502 NATR/NAST during *AMT*-19 (M. Zubkov, pers. comm.).

503 In addition to active uptake, *Trichodesmium*, which are abundant in the subtropical/
504 tropical North Atlantic due to the delivery of atmospheric Fe (Richier et al., 2012) and P
505 (Ridame et al., 2003), can scavenge both Fe (Rubin et al., 2011) and P from solution
506 (Sañudo-Wilhelmy et al., 2001). Could the same removal mechanism be an important sink
507 for Co? Although we do not have particulate Co or TdCo data for *AMT*-19, TdCo was
508 determined in surface samples (7 m depth) on *AMT*-3 (a similarly grye-centred AMT; Bowie
509 et al., 2002), where low concentrations of ~ 30 pM dCo (*AMT*-19) and TdCo (*AMT*-3) were
510 observed between 3 and 17 °N. In addition, recent studies of particulate Co in the Atlantic

511 Ocean, demonstrated that it was ~ 5% the concentration of dCo in a full-depth transect along
512 ~12 °S (Noble et al., 2012) and 12 ± 12 in the West Atlantic (Dulaquais et al., 2014a),
513 suggesting that scavenging may only be a minor sink for Co under a range of open ocean
514 environmental conditions.

515 In addition to biological uptake and particle scavenging, even if the latter is only a
516 minor sink, dCo distributions could be influenced by dissolved organic phosphorus (DOP)
517 acquisition. The region where extremely low dCo was observed is also where chronically low
518 $PO_4$ concentrations are observed (Mather et al., 2008). In the North Atlantic gyre provinces
519 the DOP pool is 5-10 times higher than inorganic phosphorus and phytoplankton and
520 bacteria must utilise AP to acquire their essential phosphorus requirement (Mahaffey et al.,
521 2014). Zinc is the metal co-factor in the protein PhoA used for AP activity and, while Co can
522 substitute for Zn as the metal centre in PhoA (Sunda and Huntsman 1995a), the preference
523 is for Zn (Saito and Goepfert 2008). A recent study in the sub-tropical Atlantic has
524 demonstrated that Zn concentrations, which are very low in this region, could limit AP activity
525 (Mahaffey et al., 2014). Therefore, the low Co concentrations may arise from uptake by
526 cyanobacteria and also from its substitution for Zn in AP. Using Co uptake results from
527 freshwater phytoplankton grown under $PO_4$ limitation, Ji and Sherrell (2008) hypothesised,
528 that the very high demand for Co in the tropical North Atlantic may be the result of persistent
529 $PO_4$ stress in this region. However, the discovery of a calcium (Ca)-based AP (Kathuria and
530 Martiny, 2011) suggests that at least some *Prochlorococcus* ecotypes and bacteria are able
531 to bypass the need for Co in AP, which may reduce the potential for Co-Zn-P co-limitation.
532 However, field based evidence in this region clearly shows that the AP activity is limited by
533 Zn (Mahaffey et al. 2014) as a result of the extremely low dZn concentrations in the North
534 Atlantic (Conway and John, 2014; Roshan and Wu, 2015).

535 In the SATL, *Trichodesmium* is largely absent (Tyrrell et al., 2003; Schlosser et al.,
536 2013), and *Procholorococcus* abundance was lower, with maximum abundances deeper
537 than in the northern gyre provinces likely due to significantly lower dFe concentrations, and a

deeper MLD in the northern section of the SATL compared with the NATR/NAST (Figs. 4 and 5). The positive correlations between dCo and *Prochlorococcus* abundance in the South Atlantic (Fig. S2, Supplemental Material) may be linked with higher inorganic phosphorus availability, as well as higher dCo. In the South Atlantic, where atmospheric deposition is low, a combination of highly efficient internal cycling (85% of the dCo uptake rate in the SATL may be accounted for by remineralisation of organic matter, Dulaquais et al., 2014a), lateral inputs (Bown et al., 2011; Noble et al., 2012) and relatively low biological demand results in higher dCo concentrations compared with the northern gyre provinces.

The different relationship between dCo and cyanobacterial dynamics in the northern gyres and the SATL suggests that dCo availability has the potential to influence the phytoplankton community structure, or vice versa, through a complex interplay with other factors, such as Fe and inorganic phosphorus availability. However, the northern gyre provinces appear unique in the sense that biotic removal dominates and controls dCo distributions (Moffett and Ho, 1986). In future decades increased stratification and predicted increases in nitrogen supply (Behera et al., 2013) could exacerbate the disparity between the northern and southern gyres in terms of trace metal distributions as a result of proximal nutrient limitation and, thus, the potential for changes to the phytoplankton community structure.

*Low oxygen waters*

Upwelling (vertical transport) can deliver macro- and micronutrient-enriched deep water to the mixed layer of the tropical North Atlantic, although for Fe the dominant flux is from the atmosphere (Ussher et al., 2013). Using the average dCo and dFe concentrations from below the surface mixed layer of the WTRA during *AMT*-19 (64 and 421 nmol $m^{-3}$, respectively) and an upward vertical mixing rate of 14.3 m $y^{-1}$ (based on the method presented by Ussher et al., 2013 for a similar cruise track, *AMT*-16), we estimate an upward vertical mixing flux of 2.5 and 16.5 nM $m^{-2}$ $d^{-1}$ for dCo and dFe, respectively. The

564 combination of this upward vertical transport of nutrient-rich water and atmospheric supply
565 sustains relatively high algal biomass in surface waters of the tropical Atlantic (e.g., the
566 maximum chl-*a* concentration of 0.41 µg $L^{-1}$ was observed at 11.5 N at 46-50 m just above
567 the thermocline and oxycline). These high levels of primary productivity result in a large
568 amount of sinking detritus. Bacterial degradation of this detritus consumes oxygen which, in
569 turn, contributes to the development of OMZs. In the productive eastern equatorial Atlantic, a
570 broad OMZ extends from ~100–900 m depth (Karstensen et al. 2008).

571 Both high dCo and dFe have previously been reported in the oxygen deficient waters
572 of the WTRA (Bowie et al. 2002; Measures et al. 2008; Pohl et al. 2010) and during *AMT*-19
573 elevated dCo (> 60 pM) and dFe (> 0.60 nM) were observed in the OMZ of the WTRA.
574 However, while elevated dFe in the sub-surface WTRA was associated with the OMZ (150
575 µM contour positioned at depths > 40–100 m depending on latitude), elevated sub-surface
576 dCo covered a much wider depth range and was not confined to the WTRA, spilling over into
577 the SATL at depths below ~ 100 m (Fig. 4). It is unlikely that the WTRA is supplying dCo to
578 the SATL, as the two provinces are separated by the South Equatorial Current (SEC), and
579 there is no evidence of elevated dFe to the south of the upwelling zone. Rather, preferential
580 scavenging of Fe with respect to Co, in the Benguela and South Equatorial Currents (Noble
581 et al., 2012), which feed into the South Atlantic gyre, provides the most likely explanation for
582 the difference in dCo and dFe concentrations to the south of the upwelling zone.

583 During *AMT*-19, the 100 µM $O_2$ contour was observed to shoal to depths as shallow
584 as 100 m, and in the WTRA as a whole the DCM was positioned just above the 150 µM $O_2$
585 horizon. In these productive waters bacterial degradation of sinking organic particles is
586 evidenced by the apparent oxygen utilisation (AOU). Furthermore, the bacteria that consume
587 the oxygen during the bacterial degradation of particles may be an additional source of high-
588 affinity, metal binding ligands (Barbeau et al., 2001; 2003) which also retain remineralised
589 Co and Fe in solution. While a positive relationship between dFe and AOU ($r^2$ = 0.6, $p$ =
590 0.03, $n$ = 7) in the latitudinal band 1-17 °N, was observed, for dCo and AOU the relationship

591 was weak and not significant ($r^2$ = 0.2, $p$ = 0.3, $n$ = 8) (Fig. 6), suggesting that other sources
592 of Co (e.g., vertical transport, lateral advection) are relatively more important in this region.

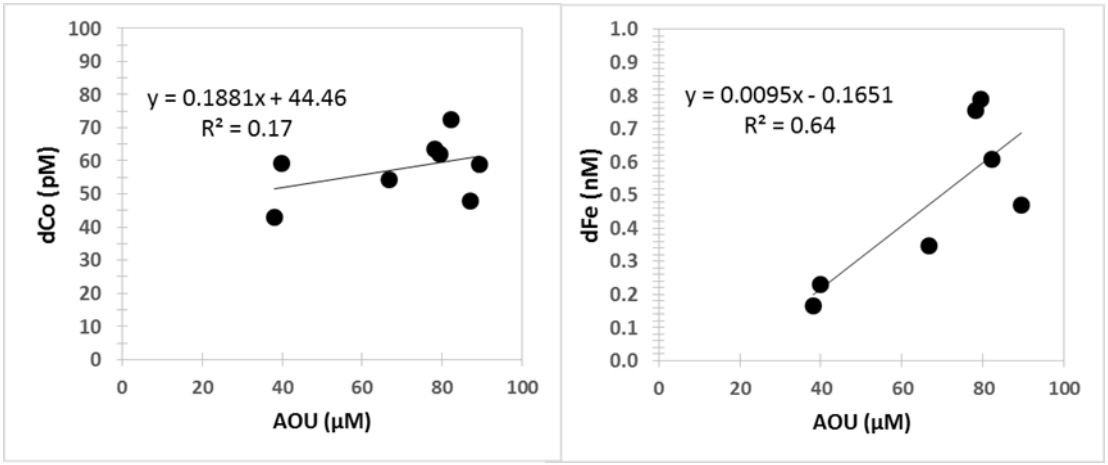


593

594 Figure 6. dCo (left) and dFe (right) plotted against the apparent oxygen utilisation (AOU; µM) in the
595 region of low dissolved oxygen (> 150 µM dissolved oxygen; 1-17 °N)

596

597 *Lateral transport*

598 In this study, surface dFe concentrations in the NADR of 0.20-0.58 nM were similar
599 to the 0.14-0.60 nM reported by Ussher et al. (2007) for Northeast Atlantic surface waters.
600 These authors observed a dFe concentration gradient over a relatively short distance
601 spanning the shelf break, and concluded that minimal lateral transport of dFe from the shelf
602 to the open ocean occurred in this region, despite severe winter storms. In this study, there
603 was little evidence for the lateral transport of dFe from the European shelf margin to the
604 open ocean. In contrast, in the NADR, a sharp gradient in dCo was observed at the
605 boundary with the NAST with the highest concentrations of dCo appearing to be transported
606 offshore along the 26.0 kg $m^{-3}$ isopycnal. In the South Atlantic, although the
607 Falkland/Malvinas Current could potentially be a vector for the offshore transport of dFe,
608 here, too, we saw no evidence for the offshore transport of dFe

609 Lateral advection may however, be a more important source of dCo. Indeed, Bown et
610 al. (2011) report evidence of just such a mechanism in the Southeast Atlantic Ocean.
611 Furthermore, Noble et al. (2012) also observed a large-scale (> 2000 km), offshore dCo
612 plume in the SATL. These authors also noted offshore advection of dFe, but that the plume
613 covered a far smaller distance (< 500 km) than the dCo plume, and despite no evidence for
614 offshore advection of dMn (a tracer for sedimentary inputs), they concluded that reducing
615 sediments on the African margin were a likely source of all three metals. However, dFe and
616 dMn were scavenged preferentially to dCo, which explained the difference in the extent of
617 the offshore plumes. Dulaquais et al. (2014b) also argue that scavenging is a fairly
618 insignificant removal term for dCo in the western Atlantic, as they were unable to resolve
619 dCo removal, via scavenging, from dilution by mixing.

620 To the south of the SATL, the cruise track passed through a dynamic frontal region,
621 the confluence of the Brazil and the Falkland/Malvinas Currents. Both western boundary
622 currents flow along the continental shelf until they meet and are deflected offshore. Indeed,
623 Boebel et al. (1999) and Jullion et al. (2010) report cross frontal mixing in the Argentine
624 Basin of the subtropical surface waters of the Brazil Current and sub-Antarctic Surface
625 Water from the Southern Ocean at the Brazil- Falkland/Malvinas confluence. Furthermore,
626 as only about 3% of fluvial Co is estimated to be retained within river systems (Sholkovitz
627 and Copland, 1981), the northward flowing Falkland/Malvinas Current may also transport
628 organically-complexed fluvial Co offshore, contributing to the elevated surface
629 concentrations in this frontal region, as has previously been reported for Fe (Rijkenberg et
630 al., 2014).

631

632 CONCLUSIONS

633 Dissolved Co and Fe distributions showed strong, and often contrasting, regional
634 differences during *AMT*-19. Extremely low concentrations of dCo (NATR/NAST; ~20-30 pM)

were observed in the northern gyre provinces where dFe was high, whereas the opposite trend was observed in the SATL. Both dCo and dFe distributions were generally nutrient-like; highlighting the nutritive role of these two bioactive elements. However, the extremely low dCo of the northern gyre provinces is somewhat of a paradox given the seemingly plentiful supply of trace elements from Saharan dust. In these regions, we propose that dCo distribution in waters shallower than ~ 100 m is controlled predominantly by biological uptake by the cyanobacteria, *Trichodesmium* and *Prochlorococcus*, and other organisms that utilise a Co analogue of AP for DOP uptake. This has important implications in the context of climate change, where stratification is predicted to increase, thus reducing phosphate inputs from below to surface waters. This situation may be further exacerbated by predicted increases in nitrogen deposition (Behera et al., 2013) as a result of increasing urbanisation/ industrialisation. Future studies should assess the potential for Co-Zn-P limitation in the North Atlantic.

While both dFe and dCo are undoubtedly supplied via the upwelling of nutrient-rich waters in the equatorial region, as evidenced by the upward vertical flux estimates, elevated dCo was not confined to the low oxygen (< 150 µM) water, reaching shallower depths and extending into the southern gyre (SATL) below depths of 100 m. We hypothesise that this broad band of elevated dCo in the WTRA and SATL is supplied and sustained by a number of mechanisms; upwelling and low oxygen concentrations (WTRA only), lateral advection, remineralisation of sinking organic material and higher solubility limits for Co compared to Fe.

The contrasting behaviour of dCo and dFe highlighted by this study provides new insights and perspectives regarding the biogeochemical cycling of Co in the Atlantic Ocean. However, further study is required to predict the impacts of different climate change scenarios, such as increased stratification and the spread of OMZs, on trace metal cycling. As such, we recommend that future AMT transects should include sampling for a suite of

bioactive trace elements to assess the potential implications for phytoplankton community dynamics.

ACKNOWLEDMENTS

With many thanks to the Captain and crew of RRS James Cook, and Carolyn Harris, Malcolm Woodward and Claire Widdicombe for kindly providing the nutrient, and the chl-*a* data, respectively. Thank you also to Mike Zubkov and Manuela Hartmann for discussion of bacterial abundance during AMT-19. We thank two anonymous reviewers for their comments and suggestions. Funding for this work was provided through a Marine Institute (Plymouth University) Studentship to RUS, a Natural Environment Research Studentship (NERC) to NJW and NERC grant number NE/G016267/1 to MCL. Thank you also to the Atlantic Meridional Transect Programme co-ordinators who provided a berth on *AMT*-19 and therefore made this study possible. This study is a contribution to the international IMBER project and was supported by the UK NERC National Capability funding to Plymouth Marine Laboratory and the National Oceanography Centre, Southampton. This is contribution number 277 of the AMT programme.

REFERENCES

Aiken, J. et al. 2000. The Atlantic Meridional Transect: overview and synthesis of data. Progress in Oceanography. 45: 257-312.

Baars, O., and Croot, P.L. 2015. Dissolved cobalt speciation and reactivity in the eastern tropical North Atlantic. Marine Chemistry. 173: 310-319.

Baker, A. R., Jickells, T. D., Witt, M., and Linge, K. L. 2006. Trends in the solubility of iron, aluminium, manganese and phosphorus in aerosol collected over the Atlantic Ocean. Marine Chemistry. 98: 43-58.

Baker, A. R., Weston, K., Kelly, S. D., Voss, M., Streu, P., and Cape, J. N. 2007. Dry and wet deposition of nutrients from the tropical Atlantic atmosphere: Links to primary productivity and nitrogen fixation. Deep Sea Research Part I: Oceanographic Research Papers. 54: 1704-1720.

691 Barbeau, K., Rue, E.L., Bruland, K.W. and Butler, A. 2001. Photochemical cycling of iron in
692 the surface ocean mediated by microbial iron(III)-binding ligands. Nature. 413: 409-413.

693 Barbeau, K., Rue, E.L., Trick, C.G., Bruland, K.W., and Butler, A. 2003. Photochemical
694 reactivity of siderophores produced by marine heterotrophic bacteria and cyanobacteria
695 based on characteristic Fe(III) binding groups. Limnology and Oceanography. 48: 1069-
696 1078.

697 Behera, S.N., Sharma, M., Aneja, V.P., and Balasubramanian, R., 2013. Ammonia in the
698 atmosphere: a review on emission sources, atmospheric chemistry and deposition on
699 terrestrial bodies. Environmental Science Pollution Research, 20, 8092-8131.

700 Bergquist, B. A., and Boyle, E.A. 2006. Dissolved iron in the tropical and subtropical Atlantic
701 Ocean. Global Biogeochemical Cycles. 20. Doi: 10.1029/2005GB002505.

702 Bertrand, E.M. et al. 2007. Vitamin $B_{12}$ and iron co-limitation of phytoplankton growth in the
703 Ross Sea. Limnology and Oceanography. 52: 1079-1093.

704 Blain, S. et al. 2007. Effect of natural iron fertilisation on carbon sequestration in the
705 Southern Ocean. Nature. 446: 1070-1074.

706 Boebel, O., Schmid, C., and Zenk, W. 1999. Kinematic elements of Antarctic Intermediate
707 Water in the western South Atlantic. Deep Sea Research Part II. 46: 355-392.

708 Bonnet, S., Webb, E.A., Panzeca, C., Karl, D.M., Capone, D.G., and Sanudo-Wilhelmy, S.A.,
709 2010. Vitamin $B_{12}$ excretion by cultures of the marine cyanobacteria Crocosphaera and
710 Synechococcus. Limnology and Oceanography, 55. Doi: 10.4319/lo.2010.55.5.1959.

711 Bowie, A.R., Whitworth, D. J., Achterberg, E. P., Mantoura, R. F. C., and Worsfold, P. J.,
712 2002. Biogeochemistry of Fe and other trace elements (Al, Co, Ni) in the upper Atlantic
713 Ocean. Deep Sea Research Part I: Oceanographic Research Papers. 49: 605-636.

714 Bown, J. et al., 2011. The biogeochemical cycle of dissolved cobalt in the Atlantic and the
715 Southern Ocean south off the coast of South Africa. Marine Chemistry. 126: 193-206.

716 Boyd, P.W., and Ellwood, M.J. 2010. The biogeochemical cycle of iron in the ocean. Nature
717 Geoscience. 3: 675-682.

718 Boyd, P. W. et al. 2007. Mesoscale iron enrichment experiments 1993-2005: synthesis and
719 future directions. Science .315: 612-617.

720 Browning, T.J., Bouman, H.A., Moore, C.M., Schlosser, C., Tarran, G.A., Woodward, E.M.S.,
721 and Henderson, G.M., 2014. Nutrient regimes control phytoplankton ecophysiology in the
722 South Atlantic. Biogeosciences, 11, 463-479.

723 Bruland, K. W. and Lohan, M.C. 2003. Controls of trace metals in seawater. In: The
724 Oceans and Marine Geochemistry. Treatise on Geochemistry vol.6. (ed. H. Elderfield), pp
725 23-47. Oxford: Elsevier.

726 Buck, C. S., Landing, W.M., Resing, J.A. and Measures, C.I. 2010. The solubility and
727 deposition of aerosol Fe and other trace elements in the North Atlantic Ocean: Observations
728 from the A16N CLIVAR/$CO_2$ repeat hydrography section. Marine Chemistry. 120: 57-70.

729 Buck, K.N., Sohst, B., and Sedwick, P.N., 2015. The organic complexation of dissolved iron
730 along the U.S.GEOTRACES (GA03) North Atlantic Section. Deep Sea Research II, 116,
731 152-165.

732 Carritt, D.E. and Carpenter, J.H. 1966. Comparison and evaluation of currently employed
733 modifications of the Winkler method for determining dissolved oxygen in seawater; a
734 NASCO Report. Journal of Marine Research. 24: 286-319.

735 Chance, R., Jickells, T.D., and Baker, A.R. 2015. Atmospheric trace metal concentrations,
736 solubility and deposition fluxes in remote marine air over the south-east Atlantic. Marine
737 Chemistry. Doi: 10.1016/j.marchem.2015.06.028.

738 Conway, T. M., and John, S.G. 2014. The biogeochemical cycling of zinc and zinc isotopes
739 in the North Atlantic Ocean."Global Biogeochemical Cycles. 28: 1111-1128.

740 Coale, K. H. et al. 1996. A massive phytoplankton bloom induced by an ecosystem-scale
741 iron fertilzation experiement in the equatorial Pacific Ocean. Nature. 383: 495-501.

742 Croot, P.L., and Heller, M.I., 2012. The importance of kinetics and redox in the
743 biogeochemical cycling of iron in the surface ocean. Frontiers in Microbiology, 3. Doi:
744 10.3389/fmicb.2012.00219.

745 Croot, P.L., Streu, P., Baker, A.R., 2004. Short residence time for iron in surface seawater
746 impacted by atmospheric dry deposition from Saharan dust events. Geophysical Research
747 Letters, 31. Doi: 10.1029/2004gl020153.

748 de Baar, H. J. W. et al. 2008. Titan: A new facility for ultraclean sampling of trace elements
749 and isotopes in the deep oceans in the international GEOTRACES program. Marine
750 Chemistry. 111: 4-21.

751 Doherty, O.M., Riemer, N., and Hameed, S., 2014. Role of the convergence zone over West
752 Africa in controlling Saharan mineral dust load and transport in the boreal summer. Tellus B,
753 66. Doi: 10.3402/tellusb.v66.23191.

754 Donat, J.R., and Bruland, K.W. 1988. Direct determination of dissolved cobalt and nickel in
755 seawater by differential pulse cathodic stripping voltammetry preceded by adsorptive
756 collection of cyclohexane-1,2-dione dioxime complexes. Analytical Chemistry. 60: 240-244.

757 Duce, R. A., et al. 1991. The atmospheric input of trace species to the world ocean. Global
758 Biogeochemical Cycles. 5, 193-259.

759 Duce, R.A., and Tindale, N.W. 1991. Atmospheric transport of iron and its deposition to the
760 ocean. Limnology and Oceanography. 36: 1715-1736.

761 Dulaquais, G. et al. 2014a. Contrasting biogeochemical cycles of cobalt in the surface
762 western Atlantic Ocean. Global Biogeochemical Cycles. 28. Doi: 10.1002/2014GB004903.

763 Dulaquais, G., Boye, M., Rijkenberg, M.J.A., and Carton, X. 2014b. Physical and
764 remineralization processes govern the cobalt distribution in the deep western Atlantic Ocean.
765 Biogeosciences. 11: 1561-1580.

766 Durand, M.D., Olson, R.J., and Chisholm, S.W. 2001. Phytoplankton population dynamics at
767 the Bermuda Atlantic time-series station in the Sargasso Sea. Deep Sea Research II. 48:
768 1983-2003.

769 Ellwood, M. J., and van den Berg, C.M.G. 2001. Determination of organic complexation of
770 cobalt in seawater by cathodic stripping voltammetry."Marine Chemistry. 75: 33-47.

771 Evangelista, H. et al. 2010. Inferring episodic atmospheric iron fluxes in the western South
772 Atlantic. Atmospheric Environment. 44: 703-712.

773 Fitzsimmons, J. N., Zhang, R., and Boyle, E.A. 2013. Dissolved iron in the tropical North
774 Atlantic Ocean. Marine Chemistry. 154: 87-99.

775 Gong, N., Chen, C., Xie, L., Chen, H., Lin, X., and Zhang, R. 2005. Characterization of a
776 thermostable alkaline phosphatase from a novel species *Thermus yunnanensis sp. nov.* and
777 investigation of its cobalt activation at high temperature. Biochimica Biophysica Acta. 1750:
778 103-111.

779 Grashoff, K., Erhardt, M., and Kremling, K. 1983. Methods in Seawater Analyses. Weinheim:
780 Verlag Chemie.

781 Hartmann, M., Gomez-Pereira, P., Grob, C., Ostrowski, M., Scanlan, D.J., and Zubkov, M.V.
782 2014. Efficient $CO_2$ fixation by surface *Prochlorococcus* in the Atlantic Ocean. ISME J 8:
783 2280-2289.

784 Hastenrath, S., and Merle, J. 1987. Annual cycle of subsurface thermal structure in the
785 tropical Atlantic Ocean. Journal of Pysical Oceanography. 17: 1518-1538.

786 Hatta, M., Measures, C.I., Wu, J., Roshan, S., Fitzsimmons, J.N., Sedwick, P., and, Morton,
787 P., 2014. An overview of dissolved Fe and Mn Distributions during the 2010–2011 U.S.
788 GEOTRACES north Atlantic Cruises: GEOTRACES GA03. Deep Sea Research Part II.
789 116:117-129.

790 Heller, M.I., Gaiero, D. M., and Croot, P. L., 2013. Basin scale survey of marine humic
791 fluorescence in the Atlantic: Relationship to iron solubility and $H_2O_2$. Global Biogeochemical
792 Cycles, 27, 88-100.

793 Helmers, E., and Schrems, O.1995. Wet deposition of metals to the tropical North and the
794 South Atlantic Ocean. Atmospheric Environment. 29: 2475-2484.

795 Heywood, J.L., Zubkov, M.V., Tarran, G.A., Fuchs, B.M., and Holligan, P.M. 2006.
796 Prokaryoplankton standing stocks in oligotrophic gyre and equatorial provinces of the
797 Atlantic Ocean: Evaluation of inter-annual variability. Deep Sea Research Part II. 53: 1530-
798 1547.

799 Ji, Y., and Sherrell, R.M. 2008. Differential effects of phosphorus limitation on cellular metals
800 in Chlorella and Microcystis. Limnology and Oceanography 53: 1790-1804.

801 Jickells, T.D., et al. 2005. Global iron connections between desert dust, ocean
802 biogeochemistry and climate. Science. 308: 67-71.

803 Johnson, K. S., Gordon, R. M. and Coale, K. H. 1997. What controls dissolved iron
804 concentrations in the world ocean? Marine Chemistry. 57: 137-161.

805 Jullion, L., Heywood, K.J. Naveira Garabato, A C. and Stevens, D.P. 2010. Circulation and
806 water mass modification in the Brazil-Malvinas Confluence. Journal of Physical
807 Oceanography. 40: 845–864.

808 Karstensen, J., Stramma, L. and Visbeck, M. 2008. Oxygen minimum zones in the eastern
809 tropical Atlantic and Pacific Oceans. Progress in Oceanography. 77: 331-350.

810 Kathuria, S., and Martiny, A.C., 2011. Prevalence of a calcium-based alkaline phosphatase
811 associated with the marine cyanobacterium Prochlorococcus and other ocean bacteria.
812 Environmental Microbiology, 13, 74-83.

813 Knauer, G.A., Martin, J.H. and Gordon, R.M. 1982. Cobalt in north-east Pacific waters.
814 Nature. 297: 49-51.

815 Kaufman, Y. J., Koren, I., Remer., L.A., Tanré, D., Ginoux, P., and Fan, S. 2005. Dust
816 transport and deposition observed from the Terra-Moderate Resolution Imaging
817 Spectroradiometer (MODIS) spacecraft over the Atlantic Ocean. Journal of Geophysical
818 Research. 110. Doi:10.1029/2003JD004436

819 Kim, G., and, Church, T.M., 2002. Wet deposition of trace elements and radon daughter
820 systematics in the South and equatorial Atlantic atmosphere. Global Biogeochem. Cycles,
821 16. Doi: 10.1029/2001gb001407.
822 Küpper, H. et al. 2008. Iron limitation in the marine cyanobacterium Trichodesmium reveals
823 new insights into regulation of photosynthesis and nitrogen fixation. New Phytologist 179:
824 784-798.
825 Laes, A. et al. 2007. Sources and transport of dissolved iron and manganese along the
826 continental margin of the Bay of Biscay. Biogeosciences. 4: 181-194.
827 Liu, X., and Millero, F.J., 2002. The solubility of iron in seawater. Marine Chemistry, 77, 43-
828 54.
829 Lohan, M. C., Aguilar-Islas, A. M., Franks, R. P. and Bruland, K. W. 2005. Determination of
830 iron and copper in seawater at pH 1.7 with a new commercially available chelating resin,
831 NTA Superflow. Analytica Chimica Acta. 530: 121-129.

832 Longhurst, A. 1998. Ecological Geography of the Sea. San Diego: Academic Press.

833 Mackey, K. R. M., Chien, C.-T., Post, A.F., Saito, M.A., and Paytan, A. 2015. Rapid and
834 gradual modes of aerosol trace metal dissolution in seawater. Frontiers in Microbiology. 5: 1-
835 11.

836 Mahaffey, C., Reynolds, S., Davis, C.E., and Lohan, M.C. 2014. Alkaline phosphatase
837 activity in the subtropical ocean: insights from nutrient, dust and trace metal addition
838 experiments. Frontiers in Marine Science. 1. Doi: 10.3389/fmars.2014.00073.

839 Mahowald, N. et al. 1999. Dust sources and deposition during the last glacial maximum and
840 current climate: a comparison of model results with paleodata from ice cores and marine
841 sediments. Journal of Geophysical Research. 104:15895–916.

842 Martin, J. H. and Gordon, R.M. 1988. Northeast Pacific iron distributions in relation to
843 phytoplankton productivity. . Deep-Sea Research. 35: 177-196.

844 Martin, J. H. 1990. Glacial-interglacial $CO_2$ change: the iron hypothesis. Paleoceanography.
845 5: 1-13.

846 Mather, R. L. et al. 2008. Phosphorus cycling in the North and South Atlantic Ocean
847 subtropical gyres. Nature Geoscience 1: 439-443.

848 Mawji, E., Gledhill, M., Milton, J.A., Tarran, G.A., Ussher, S., Thompson, A., Wolff, G.A.,
849 Worsfold, P.J., and Achterberg, E.P., 2008. Hydroxamate Siderophores: Occurrence and
850 Importance in the Atlantic Ocean. Environmental Science & Technology, 42, 8675-8680.

851 Measures, C.I., Landing, W.M., Brown, M.T. and Buck, C.S. 2008. High-resolution Al and Fe
852 data from the Atlantic Ocean CLIVAR-$CO_2$ repeat hydrography A16N transect: extensive
853 linkages between dust and upper ocean geochemistry. Global Biogeochemical Cycles. 22.
854 Doi: 10.1029/2007GB003042.

855 Mémery, L. et al. 2000. The water masses along the western boundary of the south and
856 equatorial Atlantic. Progress in Oceanography. 47: 69-98.

857 Millero, F., Yao, W., and Aicher, J. 1995. The speciation of Fe(II) and Fe(III) in natural
858 waters. Marine Chemistry. 50: 21-39.

859 Moffett, J.W., and Ho, J. 1996. Oxidation of cobalt and manganese in seawater via a
860 common microbially catalyzed pathway. Geochimica et Cosmochimica Acta. 60: 3415-3424.

861 Moore, C. M. et al. 2013. Processes and patterns of oceanic nutrient limitation. Nature
862 Geoscience. 6: 701-710.

863 Moore, C.M., Mills, M.M., Milne, A., Langlois, R., Achterberg, E.P., Lochte, K., Geider, R.J.,
864 and La Roche, J., 2006. Iron limits primary productivity during spring bloom development in
865 the central North Atlantic. Global Change Biology. 12,, 626-634.

866 Moore, J. K., Doney, S. C., Glover, D. M. and Fung, I. Y. 2002. Iron cycling and nutrient-
867 limitation patterns in surface waters of the World Ocean.Deep Sea Research: Part II: Topical
868 Studies in Oceanography. 49: 463-507.

869 Morel, F. M. M., Reinfelder, J.R., Roberts, S.B., Chamberlain, C.P., Lee, J.G. and Yee, D.
870 1994. Zinc and carbon co-limitation of marine phytoplankton. Nature. 369: 740-742.

871 Morel, F. M. M. and Price, N.M. 2003. The biogeochemical cycles of trace metals in the
872 oceans. Science. 300: 944-947.

873 Nielsdottir, M. C., Moore, C.M., Sanders, R., Hinz, D.J., and Achterberg, E.P. 2009. Iron
874 limitation of the post bloom phytoplankton communities in the Iceland Basin. Global
875 Biogeochemical Cycles. 23. Doi: 10.1029/2008GB003410.

876 Noble, A.E., Saito, M.A., Maiti, K. and Benitez-Nelson, C., 2008. Cobalt, manganese, and
877 iron near the Hawaiian Islands: a potential concentrating mechanism for cobalt within a
878 cyclonic eddy and implications for the hybrid-type trace metals. Deep Sea Research. Part II.
879 55: 1473-1490.

880 Noble, A. E. et al. 2012. Basin-scale inputs of cobalt, iron, and manganese from the
881 Benguela-Angola front to the South Atlantic Ocean. Limnology and Oceanography. 57: 989-
882 1010.

883 Obata, H., Karatani, H. and Nakayama, E. 1993. Automated determination of iron in
884 seawater by chelating resin concentration and chemiluminescence detection. Analytical
885 Chemistry. 65: 1524-1528.

886 Pohl, C., Croot, P. L., Hennings, U., Daberkow, T., Budeus, G. and Rutgers van der Loeff,
887 M. 2010. Synoptic transects on the distribution of trace elements (Hg, Pb, Cd, Cu, Ni, Zn,
888 Co, Mn, Fe, and Al) in surface waters of the Northern and Southern East Atlantic. Journal of
889 Marine Systems. 84: 24-41.

890 Powell, C.F., Baker, A.R., Jickells, T.D., Bange, H.W., Chance, R.J., Yodle, C., , 2015.
891 Estimation of the atmospheric flux of nutrients and trace metals to the eastern tropical North
892 Atlantic Ocean. Journal of the Atmospheric Sciences, 4029-4045.

893 Prospero, J. M., and Carlson, T.N. 1972. Vertical and areal distribution of Saharan dust over
894 the Equatorial North Atlantic Ocean. Journal of Geophysical Research. 77: 5255-5265.

895 Prospero, J. M., Ginoux, P., Torres, O., Nicholson, S.E. and Thomas, T.E. 2002.
896 Environmental characterization of global sources of atmospheric dust identified with the
897 Nimbus 7 Total Ozone Mapping Spectrometer (TOMS) absorbing aerosol product. Reviews
898 of Geophysics. 40. Doi: 10.1029/2000RG000095.

899 Richier, S., Macey, A.I., Pratt, N.J., Honey, D.J., Moore, C.M., and Bibby, T,S., 2012.
900 Abundances of iron-binding photosynthetic and nitrogen-fixing proteins of Trichodesmium
901 both in culture and in situ from the North Atlantic. PLoS ONE, 7. Doi:
902 10.1371/journal.pone.0035571.

903 Ridame, C., Moutin, T., and Guieu, C., 2003. Does phosphate adsorption onto Saharan dust
904 explain the unusual N/P ratio in the Mediterranean Sea? Oceanologica Acta, 26, 629-634.

905 Rijkenberg, M.J.A., Middag, R., Laan, P., Gerringa, L.J.A., van Aken, H.M., Schoemann, V.,
906 de Jong, J.T.M., and de Baar, H.J.W., 2014. The distribution of dissolved iron in the West
907 Atlantic Ocean. PLoS ONE, 9. Doi: 10.1371/journal.pone.0101323.

908 Rijkenberg, M.J.A., Steigenberger, S., Powell, C.F., van Haren, H., Patey, M.D., Baker, A.R.,
909 and Achterberg, E.P., 2012. Fluxes and distribution of dissolved iron in the eastern (sub-)
910 tropical North Atlantic Ocean. Global Biogeochemical Cycles. 26. Doi:
911 10.1029/2011gb004264.

912 Robinson, C. 2006. The Atlantic Meridional Transect (AMT) Programme: A contextual view
913 1995-2005. Deep Sea Research. Part II: Topical Studies in Oceanography. 53: 1485-1515.

914 Rodriguez, I.B., and Ho,T.-Y. 2015. Influence of Co and $B_{12}$ on the growth and nitrogen
915 fixation of *Trichodesmium*. Frontiers in Microbiology 6. Doi: 10.3389/fmicb.2015.00623.

916 Roshan, S., and Wu, J. 2015. Water mass mixing: The dominant control on the zinc
917 distribution in the North Atlantic Ocean. Global Biogeochemical Cycles. 29: 1060-1074.

918 Rubin, M., Berman-Frank, I., Shaked, Y. 2011. Dust-and mineral-iron utilization by the
919 marine dinitrogen-fixer *Trichodesmium*. Nature Geoscience, 4:529-534.

920 Rudnick, R.L., and Gao, S., 2003. Composition of the continental crust. In H.D. Holland, and
921 Turekian, K.K. (Ed.), Treatise on Geochemistry (pp. 1-64). Oxford: Elsevier.

922 Rue, E. L., and Bruland, K.W. 1995. Complexation of iron (III) by natural organic ligands in
923 the Central North Pacific as determined by a new competiative ligand equilibrium/ adsorptive
924 cathodic stripping voltammetric method. Marine Chemistry. 50: 117-138.

925 Saito, M. A. and Goepfert, T. J. 2008. Zinc-cobalt colimitation of *Phaeocystis antarctica*.
926 Limnology and Oceanography. 53: 266-275.

927 Saito, M. A., Goepfert, T.J., Ritt, J.T. 2008. Some thoughts on the concept of colimitation:
928 Three definitions and the importance of bioavailability. Limnology and Oceanography. 53:
929 276-290.

930 Saito, M. A., and Moffett, J.W. 2001. Complexation of cobalt by natural organic ligands in the
931 Sargasso Sea as determined by a new high-sensitivity electrochemical cobalt speciation
932 method suitable for open ocean work. Marine Chemistry. 75: 49-68.

933 Saito, M.A., and Moffett, J.W. 2002. Temporal and spatial variability of cobalt in the Atlantic
934 Ocean. Geochimica et Cosmochimica Acta. 66, 1943-1953.

935 Saito, M.A., Moffett, J.W., Chisholm, S. and Waterbury, J.B. 2002. Cobalt limitation and
936 uptake in *Prochlorococcus*. Limnology and Oceanography .47: 1629-1636.

937 Saito, M.A., Rocap, G. and Moffett J.W. 2005. Production of cobalt binding ligands in a
938 *Synechococcus* feature at the Costa Rica upwelling dome. Limnology and Oceanography.
939 50: 279-290.

940 Sanudo-Wilhelmy, S.A., Kustka, A.B., Gobler, C.J., Hutchins, D.A., Yang, M., Lwiza, K.,
941 Burns, J., Capone, D.G., Raven, J.A., Carpenter, E.J., 2001. Phosphorus limitation of
942 nitrogen fixation by *Trichodesmium* in the central Atlantic Ocean. Nature, 411, 66-69.

943 Sarthou, G. et al. 2003. Atmospheric iron deposition and sea-surface dissolved iron
944 concentrations in the eastern Atlantic Ocean. Deep Sea Research. Part I: Oceanographic
945 Research Papers. 50: 1339-1352.

946 Sarthou, G. et al. 2007. Influence of atmospheric inputs on the iron distribution in the
947 subtropical North-East Atlantic Ocean. Marine Chemistry. 104: 186-202.

948 Schlosser, C. et al. 2013. Seasonal ITCZ migration dynamically controls the location of the
949 (sub)tropical Atlantic biogeochemical divide. Proceedings of the National Academy of
950 Sciences. Doi: 10.1073/pnas.1318670111.

951 Shaked, Y., and Lis, H., 2012. Dissassembling iron availability to phytoplankton. Frontiers in
952 Microbiology, 3. Doi: 10.3389/fmicb.2012.00123.

953 Shelley, R. U., Morton, P.L., and Landing, W.M. 2015. Elemental ratios and enrichment
954 factors in aerosols from the US-GEOTRACES North Atlantic transects. Deep Sea Research.
955 Part II: Topical Studies in Oceanography. 116: 262-272.

956 Shelley, R. U. et al. 2012. Controls on dissolved cobalt in surface waters of the Sargasso
957 Sea: Comparisons with iron and aluminum. Global Biogeochemical. Cycles. 26. Doi:
958 10.1029/2011gb004155.

959 Shelley, R. U., Zachhuber, B. Sedwick, P.J., Worsfold, P.J. and Lohan, M.C. 2010.
960 Determination of total dissolved cobalt in UV-irradiated seawater using flow injection with
961 chemiluminescence detection. Limnology and. Oceanography: Methods. 8: 352-362.

962 Sholkovitz, E.R., and Copland, D. 1981. The coagulation, solubility and adsorption properties
963 of Fe, Mn, Cu, Ni, Cd, Co and humic acids in a river water. Geochimica et Cosmochimica
964 Acta. 45: 181-189.

965 Sultan, B., and Janicot, S. 2000. Abrupt shift of the ITCZ over West Africa and intra-seasonal
966 variability. Geophysical Research Letters. 27: 3353-3356.

967 Sunda, W.G. and Huntsman, S.A. 1995a. Cobalt and zinc inter-replacement in marine
968 phytoplankton: biological and geochemical implications. Limnology and Oceanography. 40:
969 1404-1417.

970 Sunda, W. G., and Huntsman, S.A.1995b. Iron uptake and growth limitation in oceanic and
971 coastal phytoplankton. Marine Chemistry. 50: 189-206.

972 Tarran, G.A., Heywood, J.L. and Zubkov, M.V. 2006. Latitudinal changes in the standing
973 stocks of nano- and picoeukaryotic phytoplankton in the Atlantic Ocean. Deep Sea
974 Research. Part II. 53: 1516-1529.

975 Thuroczy, C.-E., Boye, M., and Losno, R., 2010. Dissolution of cobalt and zinc from natural
976 and anthropogenic dusts in seawater. Biogeosciences, 7, 1927-1936.

977 Timmermans, K.R., Snoek, J., Gerringa, L.J.A., Zondervan, I., de Baar, H.J.W. 2001. Not all
978 eukaryotic algae can replace zinc with cobalt: *Chaetoceros calcitrans* (Bacillariophyceae)
979 versus *Emiliania huxleyi* (Prymnesiophyceae). Limnology and Oceanography. 46: 699-703.

980 Tsamalis, C., Chédin, A., Pelon, J., and Capelle, V., 2013. The seasonal vertical distribution
981 of the Saharan Air Layer and its modulation by the wind. Atmospheric. Chemistry and.
982 Physics, 13, 11235-11257.

983 Tyrrell, T., Maranon, E., Poulton, A.J., Bowie, A.R., Harbour, D.S., and Woodward, E.M.S.,
984 2003. Large-scale latitudinal distribution of Trichodesmium spp. in the Atlantic Ocean.
985 Journal of Plankton Research., 25, 405-416.

986 Ussher, S.J. et al. 2013. Impact of atmospheric deposition on the contrasting iron
987 biogeochemistry of the North and South Atlantic Ocean. Global Biogeochemical Cycles. 27:
988 1096-1107. Doi: 10.1002/gbc.20056.

989 Ussher, S. J. et al. 2007. Distribution and redox speciation of dissolved iron on the European
990 continental margin. Limnology and Oceanography. 52: 2530-2539.

991 van den Berg, C. M. G. 1995. Evidence for organic complexation of iron in seawater. Marine
992 Chemistry. 50: 139-157.

993 Vega, M. and.van den Berg, C.M.G. 1997. Determination of cobalt in seawater by catalytic
994 adsorptive cathodic stripping voltammetry. Analytical Chemistry. 69: 874-881.

995 Welschmeyer, N.A., 1994. Fluorometric Analysis of chlorophyll a in the presence of
996 chlorophyll b and pheopigments. Limnology and Oceanography. 39: 1985-1992.

997 Wong, G.T.F., Pai, S.-C., Chung, S.-W. 1995. Cobalt in the West Philippine Sea.
998 Oceanologica Acta. 18: 631-638.

999 Woodward, E.M.S., Rees, A.P. and Stephens, J.A. 1999. The influence of the south-west
1000 monsoon upon the nutrient biogeochemistry of the Arabian Sea. Deep Sea Research: Part
1001 II. 46: 571-591.

1002 Wu, J., Boyle, E. Sunda, W., and Wen, L.-S. 2001. Soluble and colloidal iron in the
1003 oligotrophic North Atlantic and North Pacific. Science. 293: 847-849.

1004 Wu, J., Roshan, S., and Chen, G., 2014. The distribution of dissolved manganese in the
1005 tropical–subtropical North Atlantic during US GEOTRACES 2010 and 2011 cruises. Marine
1006 Chemistry, 166, 9-24.

1007 Wyatt, N. J. et al. 2014. Biogeochemical cycling of dissolved zinc along the GEOTRACES
1008 South Atlantic transect GA10 at 40°S. Global Biogeochemical Cycles. 28: 44-56.